

Ionic layered PbFCl-type compounds under high pressure

F. Decremps,* M. Fischer, A. Polian, and J. P. Itié

Physique des Milieux Condensés, Université Pierre et Marie Curie, B 77, 75252 Paris Cedex 05, France

M. Sieskind

CNRS, laboratoire PHASE, Boîte Postale 20, 67037 Strasbourg Cedex 2, France

(Received 3 August 1998; revised manuscript received 14 September 1998)

X-ray diffraction experiments under high pressure have been carried out on BaFCl, BaFBr, and BaFI that belong to the family of layered ionic crystals with the matlockite PbFCl structure. Experiments up to 30 GPa with different pressure transmitting media and different powder proportions were undertaken to determine the anisotropic stress component contribution. The bulk and linear moduli were determined for each compound and structural phase transitions have been observed near 21 and 27 GPa for BaFCl and BaFBr, respectively. The difference in bond strength due to the layered properties of these compounds results in clear differences in compressibilities along the two principal directions, perpendicular and parallel to the C_4 axis of the tetragonal matlockite structure. The anisotropic behavior of the unit-cell parameters observed under compression is attributed to the anisotropic coordination of the highly polarizable halogen anion. This phenomenon created a large static dipole at the halogen and involves an energy contribution that seems to stabilize the layered structure. [S0163-1829(99)03206-3]

I. INTRODUCTION

The alkaline-earth fluorohalides MFX , where $M = \text{Ca, Sr, Ba, Pb, or Eu}$ and $X = \text{Cl, Br, or I}$, form an important class of materials crystallizing in the PbFCl-type tetragonal structure $P4/nmm$ (Fig. 1 and Table I), also called the matlockite structure.⁶ When doped with rare-earth ions, these crystals possess the property of photostimulated luminescence. Therefore, they are used for technological applications like x-ray image plates detectors⁷ (for example, BaFBr:Eu²⁺) or as *in situ* pressure gauge for experiments with diamond anvil cells at high temperature.^{8,9}

Some previous studies¹⁰⁻¹² on several MFX compounds have shown that these crystals exhibit anisotropic properties, a direct consequence of their macroscopic layered character.¹³ Moreover, like PbI_2 or CdX_2 crystals, these layered compounds are formed by atoms bonded by ionic-type forces, which seems to *a priori* be incompatible with the formation of a layerlike crystal. In conventional covalent layered materials, all the bonding electrons are within the sheets so that the layers are bonded by van der Waals forces. The issue to be investigated here is physical origin that leads to the formation of ionic-layered substances.

The matlockite family MFX forms an interesting group of compounds exhibiting an anisotropic bonding scheme that depends, at ambient conditions, on the chemical nature of the M and X atoms. They are therefore well suited to probe the physical interatomic properties that stabilize ionic-layered structure. In the present study, a high-pressure investigation of x-ray diffraction was made on BaFX ($X = \text{Cl, Br, and I}$) up to 30 GPa. Moreover, to understand how the pressure affects the intrinsic anisotropic behavior of these compounds, different high-pressure experiments on the same crystal with various pressure transmitting media (and various sample powder/pressure transmitting medium proportion) were carried out in

order to provide some insight on the deviatoric stresses or grain-grain effects.

The principal objectives of this study were

(1) to determine the pressure response of the layered MFX crystals and to compare these results with those obtained when an atom species is replaced by another one, (2) to discuss and analyze our experimental data in terms of crystal compressibilities (taking into account the deviatoric stress effects) and to compare these data with previous experimental and theoretical studies on BaFCl, BaFBr, and BaFI, and (3) to determine the nature of the bonding that stabilizes the layered structure of ionic compounds.

II. EXPERIMENTAL PROCEDURE

Starting from high-purity materials, single crystals of MFX were grown¹⁴ by slowly cooling a molten mixture of

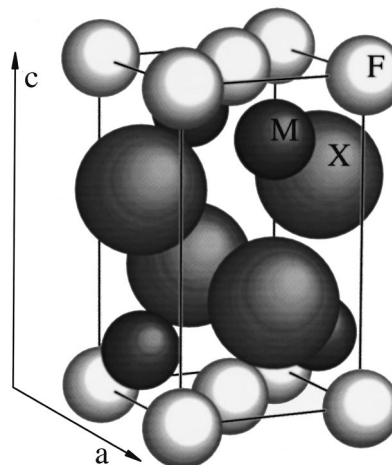


FIG. 1. An example of the matlockite tetragonal structure MFX :BaFCl (a and c are the crystallographic axes).

TABLE I. Crystal data for selected matlockite-type compounds. a and c are the lattice constants in Å, u (halogen), and u' (metal) are lattice parameters, and d_{AB} is the distance between ion A and B .

	BaFCl (Ref. 1)	BaFBr (Ref. 1)	BaFI (Ref. 1)	SrFCl (Ref. 2)	SrFBr (Ref. 3)	PbFCl (Ref. 4)	PbFBr (Ref. 5)	PbFI (Ref. 5)
a (Å)	4.394	4.508	4.654	4.126	4.218	4.110	4.18	4.23
c (Å)	7.225	7.441	7.962	6.958	7.337	7.246	7.59	8.77
u	0.6472	0.6497	0.6522	0.6489	0.6479	0.6497	0.65	0.65
u'	0.2049	0.1911	0.1704	0.2015	0.1859	0.2058	0.195	0.167
d_{FF} (Å)	3.106	3.187	3.290	2.917	2.982	2.906	3.18	3.36
d_{MF} (Å)	2.649	2.665	2.693	2.494	2.511	2.539	2.56	2.58

carefully dehydrated MX_2 and MF_2 following the chemical reaction $MX_2 + MF_2 \rightarrow 2MFX$. Because of their lamellar character, water is easily absorbed between the layers making them opaque. The crystals were therefore stored in a dessiccator and carefully selected to be fully transparent.

These studies were performed using a conventional diamond anvil cell driven by a membrane¹⁵ with diamond anvil culets of 500 μm in diameter. The stainless-steel gaskets were preindented to a thickness of 50 μm and drilled to a diameter of 150 μm . Fine powder of sample was loaded into the gasket hole. At pressures above 11 GPa (at room temperature), all pressure-transmitting media are solid and introduce anisotropic stress components that could mask the intrinsic crystal anisotropy. Therefore, in order to determine the deviatoric stress contributions, we used two different

pressure-transmitting media (silicone oil and argon) and various powder ratios during the investigation of the BaFX structure behavior. To measure the *in situ* pressure, the fluorescence emission of a ruby chip¹⁶ placed into the gasket hole was systematically recorded before and after each x-ray-diffraction experiment.

The high-pressure powder x-ray-diffraction measurements were made in the energy dispersive mode with the wiggler at the DW11 station of the DCI storage ring of the LURE (Orsay, France). After energy calibration of the detector, the 2θ angle was determined by collecting diffraction patterns of a copper sample placed between the diamonds. The polychromatic x-ray beam was collimated to a $50 \times 50\text{-}\mu\text{m}^2$ spot centered on the gasket hole. Because of the high scattering power of MFX compounds, exposure times between 20 and

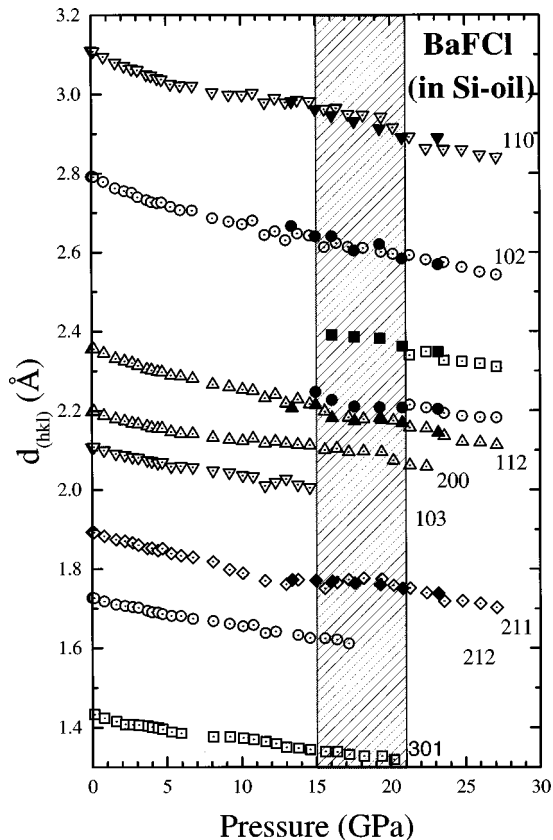


FIG. 2. Lattice spacings d_{hkl} as a function of pressure for BaFCl in silicone oil. At about 21 GPa, a phase transition takes place. Open (full) symbol: upstroke (downstroke) experimental data.

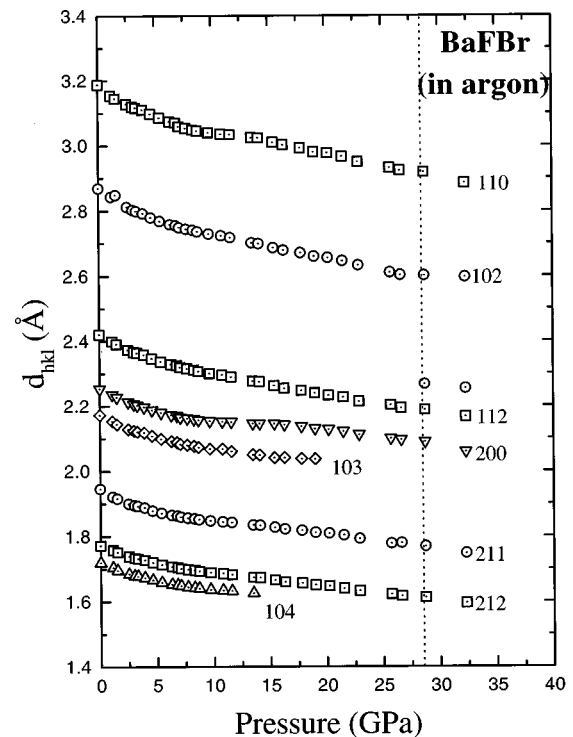


FIG. 3. Lattice spacings d_{hkl} as a function of pressure for BaFBr in argon. At about 27 GPa, a phase transition takes place.

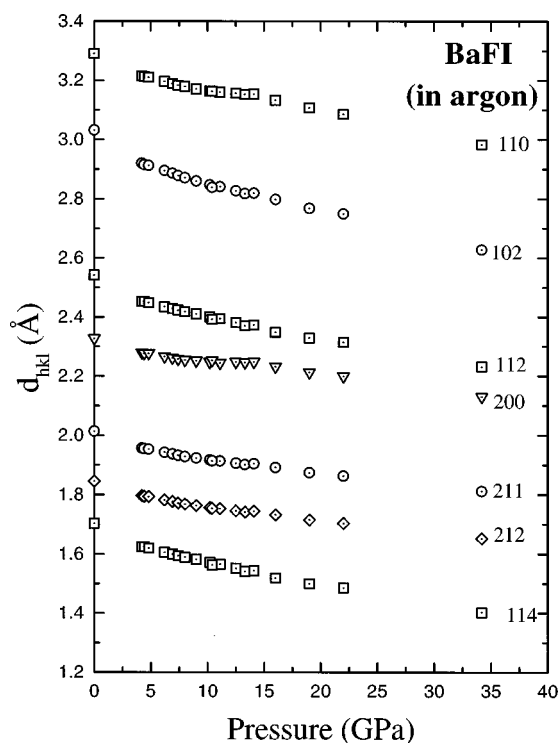


FIG. 4. Lattice spacings d_{hkl} as a function of pressure for BaFI in argon.

30 mn were sufficient to collect diffraction patterns with suitable peak-to-background intensity ratios.

III. RESULTS

A. Lattice parameters and cell volume

The unit-cell parameters a and c of the tetragonal matlockite compounds and the volume $V = a^2c$ were calculated,

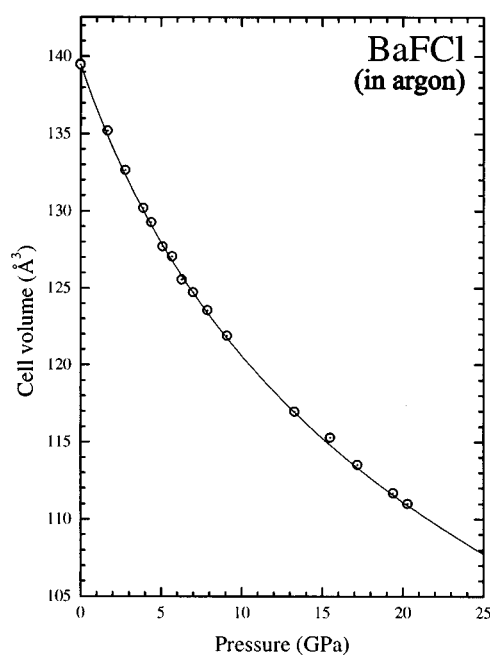
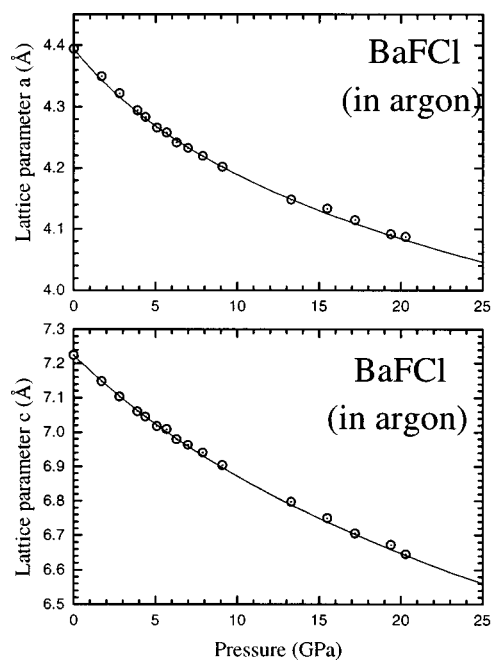


FIG. 5. Room-temperature axial and volumic compressions for BaFCl as a function of pressure. The solid curves represent the Muraghan equation of state best fit.

with a least-squares refinement program DICVOL,¹⁷ from the diffraction patterns. Peak positions were determined by a Gaussian fitting of the diffracted lines. For the complete set of compounds, at least seven intense diffracted lines were selected up to the maximum pressure achieved and used in the refinement (see Figs. 2–4 for BaFCl, BaFBr, and BaFI, respectively).

Variations, sometimes large, of the diffraction linewidths were observed in different runs with two different pressure-transmitting media (silicone oil and argon), even with approximately the same small powder quantity in order to minimize the grain-grain contact effects. The effects on the compression curves due to the deviatoric stresses are discussed in Appendix A.

Finally, the accurate values of the unit-cell parameters a , c , and cell volume V of BaFCl, BaFBr, and BaFI are given as a function of pressure in Figs. 5–7 respectively.

For the three crystals studied, the normalized volume V/V_0 , where V_0 is the cell volume at ambient conditions, is plotted as a function of the pressure in Fig. 8.

B. Phase transition

At 21 GPa for BaFCl and 27 GPa for BaFBr, the appearance of new diffraction peaks reflects the occurrence of a phase transition, in good agreement with the previous high-pressure study made by Shen *et al.*¹⁰ or Subramanian *et al.*¹⁸ These transitions are confirmed by Raman scattering obtained on single crystals of BaFCl, BaFBr, and BaFI using nitrogen as the pressure-transmitting medium,¹⁹ where the phase transitions were observed at 21, 27, and 55 GPa, respectively. Unfortunately, in the best cases, only two new lines corresponding to the d spacing of the new structure were available and the high-pressure structure could not be identified without ambiguities. Results recently published by Subramanian *et al.*¹⁸ allowed us to analyze our spectra above the transition pressure, with the assumption that all the peaks

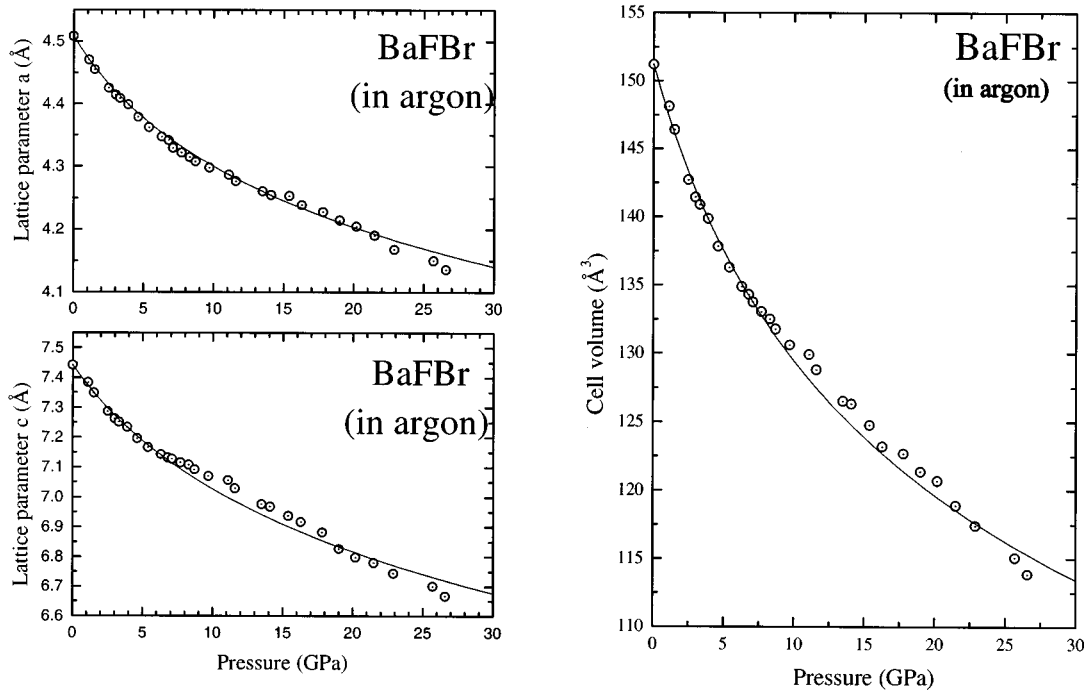


FIG. 6. Room-temperature axial and volumic compressions for BaFBr as a function of pressure. The solid curves represent the Murnaghan equation of state best fit.

come from the high-pressure phase. Our data agree with several monoclinic structures including the $P2_1/m$ one proposed in this paper. However, we cannot exclude a possible phase mixture above 21 GPa for BaFCl or 27 GPa for BaFBr, suggesting large kinetics effects for the phase change at ambient temperature.

Three different experiments were made on BaFBr up to about 30 GPa with different quantities of powder and

pressure-transmitting media. Because we observed the phase transition at 27 GPa in the three runs, we conclude that it is not affected by the deviatoric stresses. On the other hand, the intensity and the width of the new diffraction peaks (observed above 27 GPa) depend on the pressure-transmitting medium and the changes in diffraction patterns were more pronounced in silicone oil than in argon. The experiment on BaFCl in argon were only performed up to 20.2 GPa and

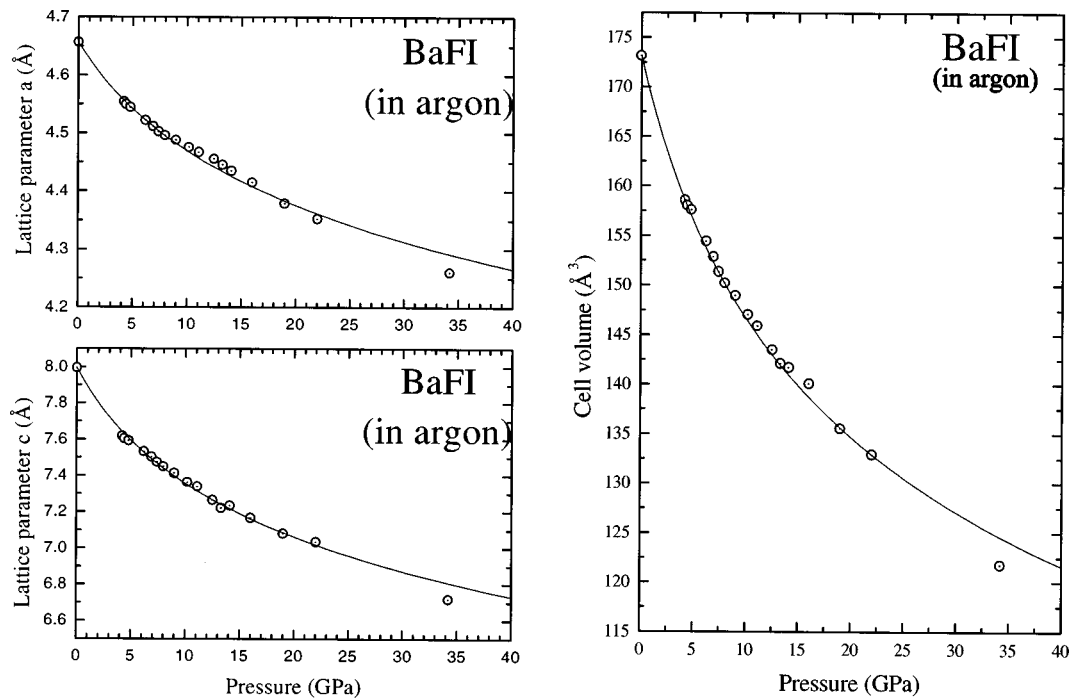


FIG. 7. Room-temperature axial and volumic compressions for BaFI as a function of pressure. The solid curves represent the Murnaghan equation of state best fit.

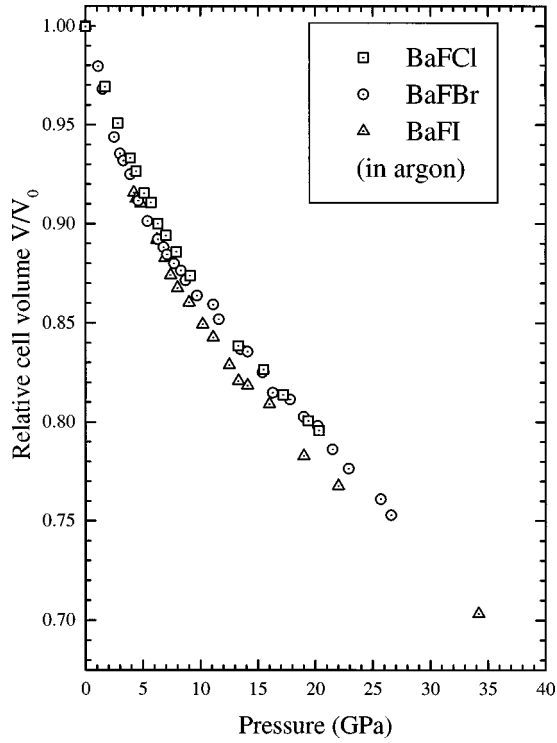


FIG. 8. Variation of the relative volume of BaFX ($X=\text{Cl}$, Br, and I) as a function of pressure. Notice the small difference of the compression curve for the three different compounds with different degrees of layering.

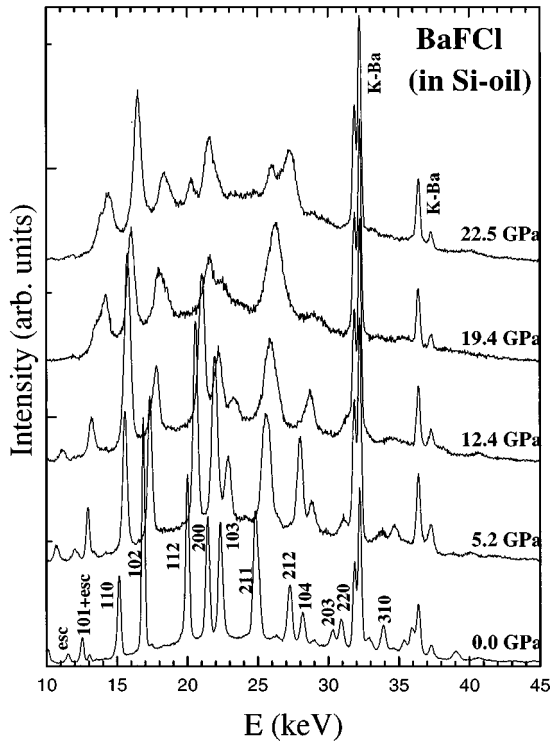


FIG. 9. Energy dispersive x-ray-diffraction spectra for BaFCl in silicon oil at different pressures above and below the phase transition one. esc and $K\text{-Ba}$ refer to the escape peaks and the fluorescence lines of Ba, respectively. The value of the Bragg angle was 7.474° .

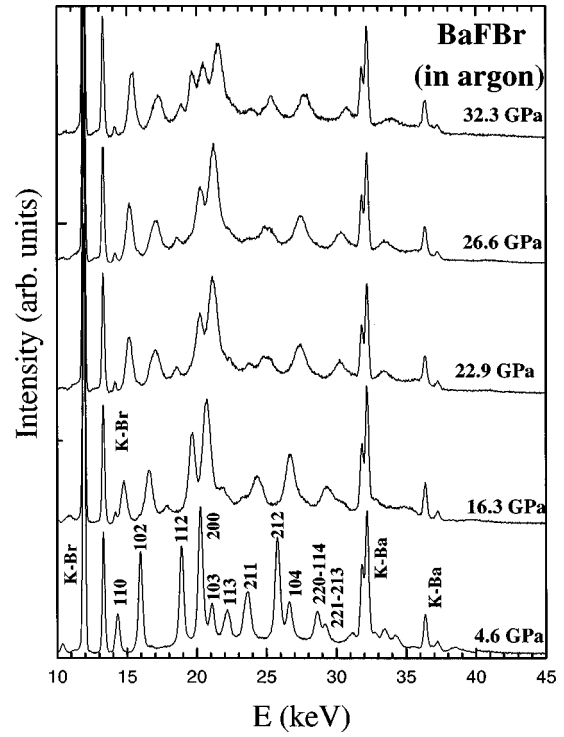


FIG. 10. Energy dispersive x-ray-diffraction spectra for BaFBr in argon at different pressures above and below the phase transition one. esc, $K\text{-Ba}$, and $K\text{-Br}$ refer to the escape peaks and the fluorescence lines of Ba and Br, respectively. The value of the Bragg angle was 8.0375° .

therefore the phase transition in this compound is illustrated in Fig. 9 by the evolution (up to 22.5 GPa) of the diffraction spectra when silicone oil was used. Figure 10 for BaFBr in argon shows these changes up to 32.3 GPa and Table II gives the values of the new diffraction peaks position for the complete set of experiments.

C. Bulk and linear moduli

The isothermal volume data determined above are fitted with a Murnaghan equation of state:²⁰

$$\frac{V}{V_0} = \left(1 + \frac{B'}{B_0} P \right)^{-1/B'}, \quad (1)$$

where V_0 is the cell volume at ambient conditions, B_0 the bulk modulus, and B' its pressure derivative.

The pressure–lattice-parameters data, $a(P)$ and $c(P)$, were fitted with a similar equation of state:²¹

$$\frac{a}{a_0} = \left(1 + \frac{B'_a}{B_a} P \right)^{-1/B'_a}, \quad (2)$$

$$\frac{c}{c_0} = \left(1 + \frac{B'_c}{B_c} P \right)^{-1/B'_c}, \quad (3)$$

where a_0 and c_0 are the room-pressure lattice parameters, B_a and B_c the linear moduli along the direction perpendicular and parallel to the tetragonal axis, respectively, and B'_a and B'_c their pressure derivatives.

TABLE II. Interplanar distances d_{hkl} (in Å) corresponding to the new diffraction peaks of the high-pressure phase of BaFCl and BaFBr. For experiments with silicone oil as pressure-transmitting media, two new peaks [$d_{hkl}(1)$ and $d_{hkl}(2)$] have been followed. P represent the pressure in GPa.

P (GPa)	BaFCl (in silicone oil)		BaFBr (in silicone oil)		BaFBr (in argon) d_{hkl} (Å)
	Upstroke $d_{hkl}(1)$ (Å)	$d_{hkl}(2)$ (Å)	$d_{hkl}(1)$ (Å)	$d_{hkl}(2)$ (Å)	
21.3	2.339	2.214			
22.4	2.348	2.207			
23.6	2.326	2.193			
24.8	2.324	2.186			
26.0	2.318	2.183			
27.1	2.310	2.182			
28.7					2.267
29.3			2.272	2.369	
32.3					2.254
Downstroke	$d_{hkl}(1)$ (Å)	$d_{hkl}(2)$ (Å)	$d_{hkl}(1)$ (Å)	$d_{hkl}(2)$ (Å)	d_{hkl} (Å)
23.2	2.348	2.203			
20.8	2.361	2.207			
19.3	2.381	2.208			
17.6	2.385	2.210			
16.1	2.390	2.226			
15.0		2.247			

From the experimental data obtained by using argon as a pressure-transmitting medium, the value of these parameters deduced for each compound are listed in Table III and the result of the best fit is plotted in Figs. 5–7.

1. BaFCl

A previous ultrasonic study of the elasticity of BaFCl single crystals under hydrostatic pressure²² yielded to B_0

$=44 \pm 5$ GPa and $B' = 5.8 \pm 0.7$, in excellent agreement with the present x-ray-diffraction results: $B_0 = 45 \pm 3$ GPa and $B' = 5.2 \pm 0.5$. These results are also consistent with shell model calculations¹² $B_0 = 41.4$ GPa or scaling factors:²⁴ $B_0 = 43.0$ GPa, and in a slight agreement with LDA (local density approximation) calculations.²³ $B_0 = 51.6$ GPa. On the other hand, our results differ significantly from those obtained by energy dispersive x-ray-diffraction experiments

TABLE III. Equation-of-state parameters of BaFX ($X = \text{Cl, Br, I}$). The calculated errors on these parameters include both volume and pressure-measurement uncertainties. ΔP corresponds to the pressure range used to determine each parameter.

Compounds	Authors	ΔP (GPa)	B_a (GPa)	B'_a	B_c (GPa)	B'_c	B_0 (GPa)	B'
BaFCl	This work ^a	21	132 ± 12	18 ± 5	139 ± 15	10 ± 4	45 ± 3	5.2 ± 0.5
	Shen ^a <i>et al.</i> (Ref. 10)	21	155 ± 10	17 ± 4	237 ± 12	0 ± 1	62 ± 6	4 ± 1
	Decremps ^b <i>et al.</i> (Ref. 11)		133 ± 13		131 ± 22		44 ± 5	5.8 ± 0.7
	Balasubramanian ^b <i>et al.</i> (Ref. 12)		105		195		41.4	
	Kalpana ^d <i>et al.</i> (Ref. 23)						51.6	4
	Sieskind ^e <i>et al.</i> (Ref. 24)			131		124		43
BaFBr	This work ^a	7	135 ± 20	19 ± 8	109 ± 20	15 ± 8	42 ± 6	6 ± 2
	Shen ^a <i>et al.</i> (Ref. 10)	27	156 ± 14	15 ± 4	121 ± 28	9 ± 2	44 ± 7	5 ± 1
	Decremps ^b <i>et al.</i> (Ref. 11)		134 ± 30		108 ± 18		41 ± 10	
	Kalpana ^d <i>et al.</i> (Ref. 23)						44.0	4
	Sieskind ^e <i>et al.</i> (Ref. 24)			118		111		38.5
BaFI	This work ^a	34	150 ± 20	22 ± 6	70 ± 10	11 ± 5	36 ± 5	6 ± 1
	Kalpana ^d <i>et al.</i> (Ref. 23)						41.2	4
	Sieskind ^e <i>et al.</i> (Ref. 24)			100		94.5		32.8

^aEnergy dispersive x-ray-diffraction experiments on powder.

^bUltrasonic and/or Brillouin scattering experiments.

^cShell-model calculations.

^dCalculations by the tight-binding linear muffin-tin-orbital method within the local-density approximation.

^eScaling factors (deduced from the shell-model formulas and from the physical properties of the fluoride MF_2).

TABLE IV. Comparison between the effect of the relative volume V/V_0 and the X anion chemical nature on the c/a ratio.

c/a		1.715	1.655	1.645
BaFCl	V/V_0			1
BaFBr	V/V_0		1	0.93
BaFI	V/V_0	1	0.86	0.85

performed by Shen *et al.*¹⁰ using ethanol:methanol:water (16:3:1) as a pressure-transmitting medium: $B_0 = 62 \pm 6$ GPa and $B' = 4 \pm 1$, where the difference on the bulk modulus is larger than 30%. More specifically, the comparison between the lattice-parameter variation $c(P)$ (linear modulus $B_c = 237 \pm 12$ GPa) of Shen *et al.*¹⁰ and our experimental data ($B_c = 139 \pm 15$ GPa, obtained using argon) clearly reveal the effect of deviatoric stresses and/or grain-grain contact that may have strongly affected the accuracy of their results.

2. BaFBr

A first-order Murnaghan equation of state was fitted to our results up to 27 GPa (phase-transition pressure), although deviatoric stresses seem to have an effect above 7 GPa (weak shrinking of the gasket hole). Contrary to BaFCl, the present results on BaFBr ($B_0 = 42 \pm 6$ GPa and $B' = 6 \pm 2$) are consistent with the values of Shen *et al.*¹⁰ $B_0 = 44 \pm 7$ GPa and $B' = 5 \pm 1$. Moreover, a combined Brillouin scattering/ultrasonic study carried out in parallel with this work¹¹ led to $B_0 = 42.5 \pm 5.0$ GPa. Good agreement is also obtained with the moduli given by the theory: Kalpana *et al.*²³ (LDA method) published $B_0 = 44.0$ GPa and Sieskind *et al.*²⁴ (scaling factor) $B_0 = 38.5$ GPa.

3. BaFI

Because of the layered nature of this crystal, we paid special attention to the experimental procedure (two samples were run instead of one as with the other two materials). The values of $B_0 = 36 \pm 5$ GPa and $B' = 6 \pm 1$ were determined by fitting a Murnaghan equation of state to the data points up to 34 GPa. No signature of a phase transition has been observed up to 34 GPa, in good agreement with the high-pressure Brillouin and Raman-scattering experiments previously performed¹⁹ (pressure transition seen at about 55 GPa). The comparison with theoretical results obtained by Kalpana *et al.*²³ ($B_0 = 41.2$ GPa and $B' = 4$) or Sieskind *et al.*²⁴ ($B_0 = 32.8$ GPa) is good.

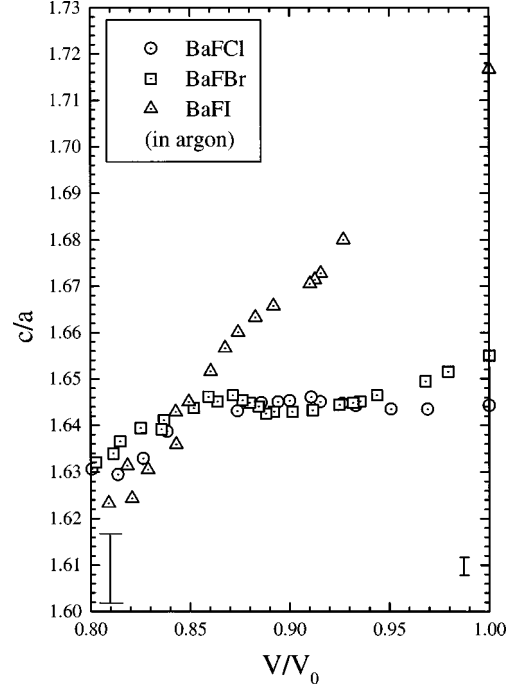


FIG. 11. Change in the ratio c/a of BaFCl (circles), BaFBr (squares), and BaFI (up triangles) with relative cell volume V/V_0 , where V_0 denotes the volume at atmospheric pressure and at room temperature. The corresponding experiments were carried out with a small powder quantity and argon as a pressure-transmitting medium. The linear variation of the uncertainties on the ratio and the relative cell volume are given by the errors bars.

D. Layer character under pressure

We have also used Eqs. (2) and (3) to calculate the linear moduli and their pressure derivatives perpendicular and parallel to the tetragonal axis (see Table III). The following inequalities demonstrate that the ratio of the linear moduli B_c/B_a decreases with increasing X anion volume:

$$\left(\frac{B_c}{B_a}\right)_{\text{BaFCl}} = 1.0 > \left(\frac{B_c}{B_a}\right)_{\text{BaFBr}} = 0.80 > \left(\frac{B_c}{B_a}\right)_{\text{BaFI}} = 0.45. \quad (4)$$

The uncertainty in the ratios is less than 5%. For BaFBr, because of the anomalies detected above 7 GPa, the linear moduli were determined by fitting the Murnaghan equation only between 0 and 7 GPa. As already mentioned, apart from BaFCl, these results are consistent with previous results obtained by x-ray-diffraction¹⁰ and ultrasonic or Brillouin-scattering techniques.^{11,22,25,26} On the other hand, our experimental results differ considerably from those calculated by Sieskind *et al.*,²⁴ who report a ratio of the linear moduli

TABLE V. Selected distances, in Å, between ions in some matlockite-type compounds at ambient pressure.

	BaFCl (Ref. 1)	BaFBr (Ref. 1)	BaFI (Ref. 1)	SrFCl (Ref. 2)	SrFBr (Ref. 3)	PbFCl (Ref. 4)	PbFBr (Ref. 5)	PbFI (Ref. 5)
$d_{M'X}$ (Å)	3.282	3.403	3.582	3.104	3.221	3.089	3.18	3.36
$d_{M''X}$ (Å)	3.194	3.409	3.844	3.110	3.387	3.216	3.45	4.30

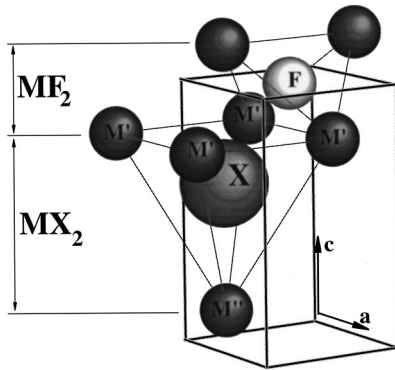


FIG. 12. Polyhedral representation of the matlockite structure. Contrary to the fluorine inside the M_4F tetrahedra, the halogen X is in a nonequidistant position from the M cations that defined the pyramid corner ($d_{M'X} \neq d_{M''X}$). (a and c are the crystallographic axes.)

B_c/B_a that does not change with the chemical nature of the ions, with a value of 0.94 for all these crystals. In fact, Sieskind discussed this result as an instructive example of the restrictive applicability of the scaling factor, where the crystals MFX are considered as quasitridimensional compounds at ambient conditions.

As shown in Appendix A, the effects of the deviatoric stresses on the pressure dependence of the c/a ratio are small when argon is used as a pressure-transmitting medium. Therefore, the pressure response of the c/a ratios (illustrated in Fig. 11) describes the evolution of the intrinsic anisotropic bonding of these compounds.²⁷ The evolution of c/a for the three compounds contrasts with the $V/V_0(P)$ curves (see Fig. 8) that are the same whatever the crystal, and therefore whatever their layer character. For BaFI, the c/a ratio strongly decreases down to $V/V_0=0.85$ (corresponding to a

TABLE VI. Computed energy polarization of BaFX crystals.

Crystals	BaFCl	BaFBr	BaFI
E_{pol} (kJ mol ⁻¹)	6.1	7.4	22.0

pressure of 15 GPa). A similar type of variation is observed for BaFBr where the layered/nonlayered transition is seen at $V/V_0=0.93$ ($P \sim 3$ GPa). Below this value, the c/a ratio seems to be constant, revealing a strengthening of the initial weak forces along the C_4 axis. On the other hand, the BaFCl c/a ratio does not exhibit a strong pressure dependence down to $V/V_0=0.85$, which is consistent with its tridimensional character.

Below $V/V_0 \approx 0.85$, all the three compounds appear to show a low decrease in c/a . However, because of the experimental error at high pressure (see error bar in Fig. 11), it is not possible to draw any reliable conclusions.

IV. COHESIVE ENERGY OF IONIC COMPOUNDS WITH LAYERED STRUCTURE

A. Polarization energy and structure stability

Table IV contains the values of the c/a ratios of BaFX as a function of the relative volume V/V_0 . From this point of view, it seems to be equivalent to replace an halogen atom X by a smaller one at ambient pressure, or to decrease the cell volume (increase the pressure) on a given compound. Therefore, to understand the structural behavior under high pressure of an ionic lamellar matlockite compound, a study at ambient pressure of the stability of several crystals belonging to this family is a convenient substitute.

The first and basic question is to understand why some crystals of this family, e.g., BaFI, have a more anisotropic

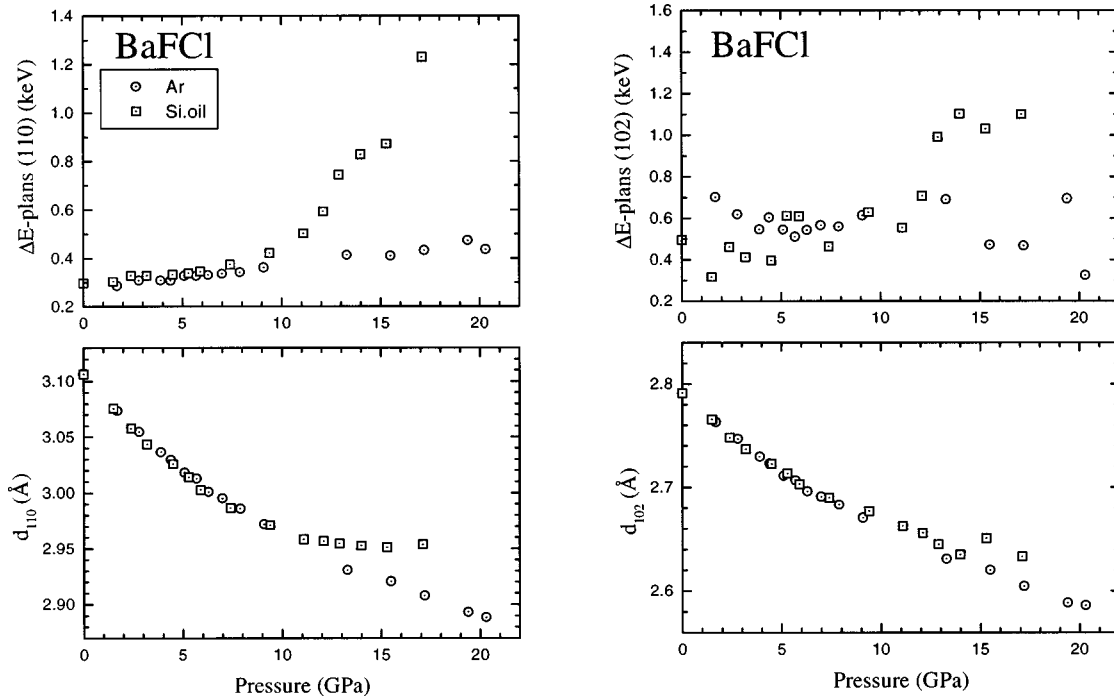


FIG. 13. Effect of two different pressure-transmitting media (silicone oil and argon) on the compression of BaFCl. A low proportion of powder was placed into the gasket hole. Circles (squares): argon (silicone oil) pressure-transmitting medium.

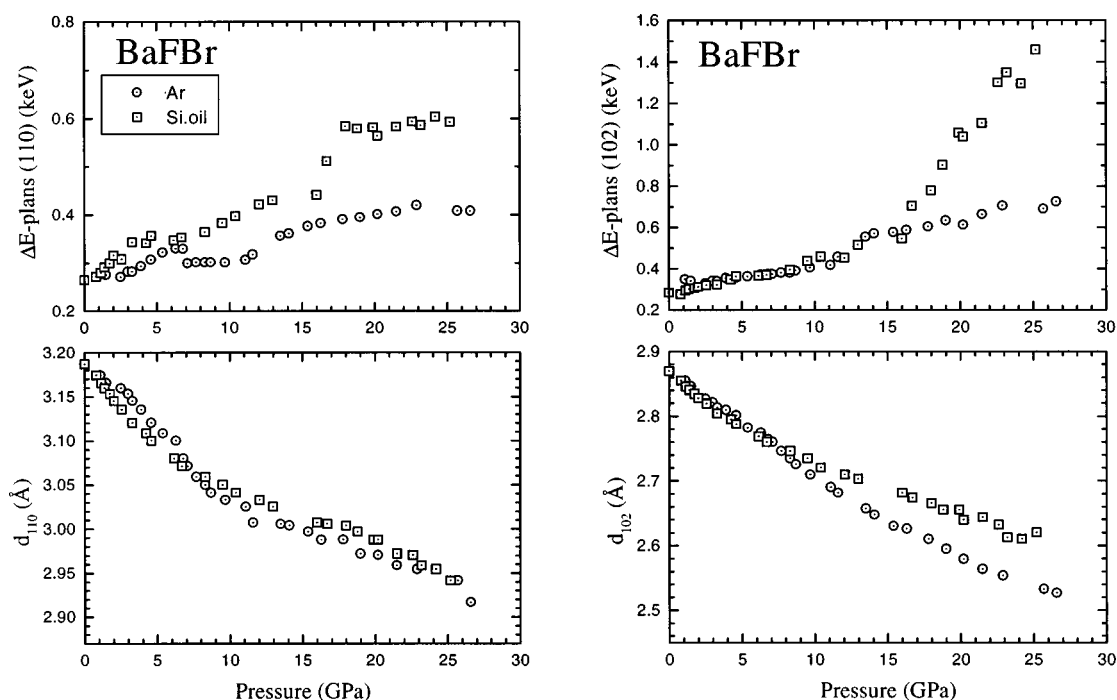


FIG. 14. Effect of two different pressure-transmitting media (silicone oil and argon) on the compression of BaFBr. A low proportion of powder was placed into the gasket hole. Circles (squares): argon (silicone oil) pressure-transmitting medium.

bonding scheme than a quasitridimensional crystal like BaFCl. The previous results have shown that the layered character of a matlockite MFX is linked to the size of the X halogen: an increase of the X -atom size tends to reduce the structure compactness. Because the electronic polarizability is directly proportional to the atomic size, we introduce the

polarizability α_x of the X halogen anion since we expect that it might be important in determining the equilibrium structure of ionic-layered compounds.

In the classical theory of ionic crystals,²⁸ the cohesive energy can be written as the sum of the Madelung and a repulsive energy:

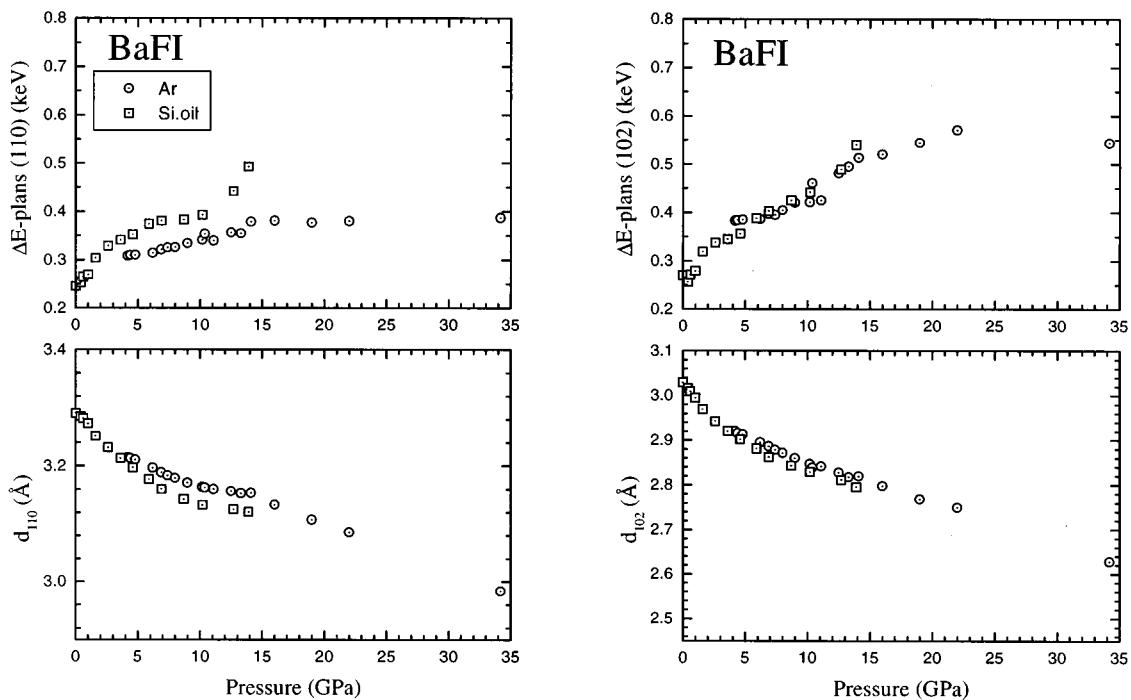


FIG. 15. Effect of two different pressure-transmitting media (silicone oil and argon) on the compression of BaFI. A low proportion of powder was placed into the gasket hole. Circles (squares): argon (silicone oil) pressure-transmitting medium.

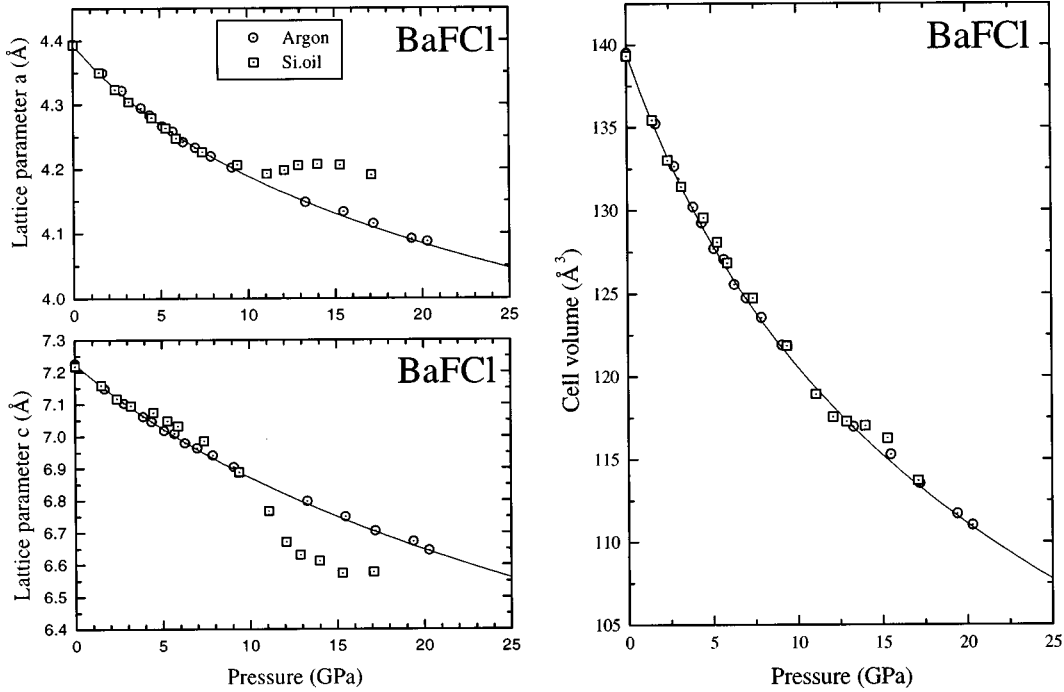


FIG. 16. BaFCl volume compression obtained with two different pressure-transmitting media (silicone oil and argon).

$$E_{\text{coh}} = E_{\text{Mad}} + E_{\text{rep}} = -\frac{NAZ^2e^2}{R} + NBR^{-n} \quad (5)$$

where N is the number of cations in the crystal, A the Madelung constant, Ze the charge of the anion, R the shortest anion-cation distance, B the repulsive constant, and n a positive integer number. It has been shown²⁹ that zero-point motions of nuclei and van der Waals forces produce only small contributions to the lattice energy and, hence, they are ignored in the discussion that follows.

For layered-ionic compounds, because of the large polarizability of the X anion (in Debye units,³⁰ $\alpha_{\text{Cl}} = 2.96$, $\alpha_{\text{Br}} = 4.16$, $\alpha_{\text{I}} = 6.43$), we may expect that electric dipole moments play an active role in their static and dynamic properties.^{31,32} In order to account for this effect, a contribution to the cohesive energy due to the local electric field \mathbf{E} on the highly polarizable X anion is included in the previous model:

$$E_{\text{coh}} = E_{\text{Mad}} + E_{\text{rep}} + E_{\text{pol}} = -\frac{NAZ^2e^2}{R} + NBR^{-n} - \frac{1}{2}N\alpha_x\mathbf{E}^2. \quad (6)$$

In a first approximation, the local electric field \mathbf{E} is determined by point charges of the neighboring ions around the X halogen. It leads to an energy contribution

$$E_{\text{pol}} = -\frac{NCZ^2e^2\alpha_x}{R^4}, \quad (7)$$

where C is a dimensionless constant that depends on the structure.

B. Application to the matlockite family

The atomic arrangement in the matlockite structure, illustrated in Fig. 12, is obtained by stacking alternate sheets of

MF_2 and MX_2 : the MF_2 sublattice is formed by corner-shared cation tetrahedra centered around a fluorine. The second sheet MX_2 is made up of edge-shared cation pyramids inside which the halogen X has an asymmetric coordination, which means that the halogen is equidistant from the four basal plane M' cations (distances $M'X$) but at a different distance from the M'' apex cation (distance $M''X$) (see Table V and Fig. 12).

A simple calculation of the local electric field inside the pyramid is proposed in Appendix B. This calculus allows to determine the variation of the C parameter as a function of the halogen position around the cations pyramid. This constant is larger for a distorted structure (like the Ba_5I pyramid of BaFI with a large asymmetric coordination of the I anions) than for a quasitridimensional compound (such as BaFCl, where the quasisymmetric coordination of Cl tends to cancel the polarization energy).

A rigorous calculation using the Bertaut method³³ of the total polarization energy for the three BaFX compounds has been also performed on the basis of Eq. (7). The result, which is summarized in Table VI, shows a strong dependence of the polarization energy with the halogen size, which is consistent with the simple calculation of the C parameter variation in Appendix B.

V. CONSEQUENCES OF THE X HALOGEN CHARACTERISTICS ON THE LAYERED PROPERTIES

The large polarizability and asymmetrical coordination of the X halogen atom allow us to understand the stability of ionic layered crystals.

(i) *Contribution of the polarization energy to the structure stability.* The structure of ionic layered compounds is stabilized by the combined effect of the halogen anisotropic coordination [increasing the C value in Eq. (7)] and the large polarizability that lead to large static dipoles on the anions

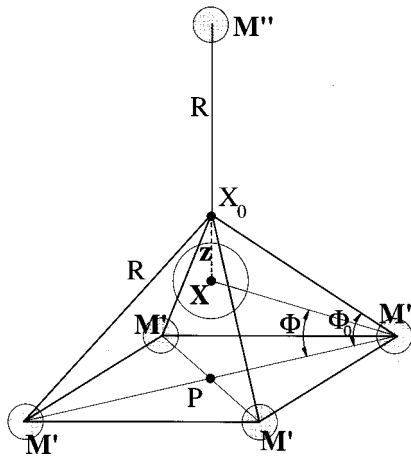


FIG. 17. Position of the halogen atom X in the cations pyramid.

and give an extra-energy term to the quasitridimensional lattice energy.

(ii) *Effect of the halogen atom polarization on the compressibilities.* In terms of stability, the considerations above show that the most favorable MFX crystal structure is obtained for an asymmetric position of highly polarizable halogen atoms. Hence, the distance between the halogen planes must be larger than for an isotropic coordination, leading to a layerlike structure. The weak bonds between the halogen planes increase the linear compressibility along C_4 . The linear compressibility perpendicular to C_4 are only due to a simple steric dimension effect, in relation to a classical ionic structure.

(iii) *Redistribution of the halogen coordination under pressure.* The anisotropic bonding forces between ions in this layered structure are related to the nonequidistant position of the halogen atom around the cations. Therefore, the pressure, which affects primarily the weak bonds, may lead to a redistribution of the halogen coordination, decreasing the C -constant value of Eq. (7) down to its minima, and, hence, causing the polarization on the halogen to vanish. In this way, the pressure evolution of the $BaFI$ c/a ratio is significant: from 0 to about 15 GPa ($V/V_0 \approx 0.83$), the strong decrease of the ratio, compared to that of $BaFCl$ or $BaFBr$, could indicate a kind of gradual layer-nonlayer transformation.

VI. CONCLUSION

The observed anisotropy of layered compounds appears to be a direct consequence of the bonding-type anisotropy inside their structures. For example, it is now well established³⁴ that the layered covalent crystals exhibit two distinct kinds of bonding, a covalent one inside the layers with van der Waals type forces between the slabs. The situation appears to be quite different for ionic-layered compounds such as $BaFX$ (which may also be right for other ionic-layered compounds like PbI_2 or CdX_2), where only one type of force is present. A layer structure for ionic crystals with large halogen atoms (high polarizability due to the large size) appears to be the most favorable framework in terms of stability. Hence, the anisotropic position of the halogen atoms modulate the magnitude of the Coulomb forces along

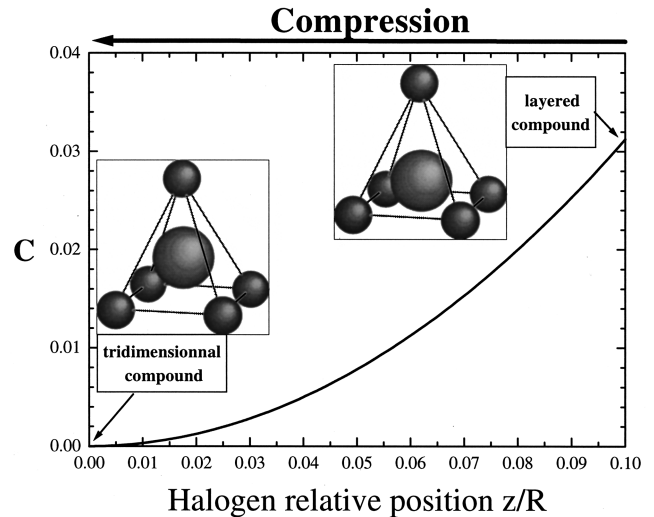


FIG. 18. Variation of the C parameter of Eq. (7) as a function of the relative halogen position in the pyramid z/R [see Eq. (B1)]. At $z/R=0$, the halogen atom is at the pyramid center of mass (X_0).

the direction parallel to the C_4 axis in order to create halogen slabs weakly bonded together. The present x-ray-diffraction experimental results allowed us to deduce and argue the assumptions above that give a new contribution to the understanding of how the pressure affects condensed matter.

ACKNOWLEDGMENTS

We would like to gratefully acknowledge Michel Gauthier and Marcos Grimsditch for helpful comments and discussions. Physique des Milieux Condensés is unité mixte de recherche n° 7602 of the CNRS.

APPENDIX A: HYDROSTATIC LIMITS OF SILICON OIL AS A PRESSURE-TRANSMITTING MEDIUM

To illustrate how the pressure-transmitting media may affect the quality of the lattice parameters determination in $BaFCl$, $BaFBr$, and $BaFI$, we report in Figs. 13–15, respectively, the pressure-width dependence of two diffraction lines (110) and (102), involving for the first one the $a(P)$ variation and, for the second one, the coupled $a(P)$ and $c(P)$ variation. We note, starting at about 10 GPa, a strong and gradual broadening of the diffraction lines when the experiment is performed with silicone oil. At the same time, a jump in the value of the lattice parameter and a broadening of the ruby line were also observed. This effect, commonly observed in high-pressure experiments (e.g., Refs. 35–37) may be ascribed to the glass transition of the pressure medium. On the other hand, no strong dependence with pressure of the diffraction linewidths was noted when argon was used. From 0 to 10 GPa, the lattice parameters obtained with the two different media are in good agreement. At higher pressure, the variation of the a and c parameters should only be discussed when the experiment was performed with argon. Surprisingly, in the whole pressure range, we noted that the shifts on these parameters due to the nonhydrostatic property of silicone oil seem to complement each other in order to give the “argon value” of the cell volume (illustrated in Fig.

16), but we cannot account for this.

We also performed experiments on BaFCl and BaFI with different quantities of powder (and with the same pressure-transmitting medium): when the gasket hole was full of powder, the experimental results were not reproducible, and did not agree with previously published data.

APPENDIX B: SIMPLE CALCULATION OF THE LOCAL ELECTRIC-FIELD VARIATION WITH THE HALOGEN POSITION

Let M'' be the apex pyramid cation, M' the corners of the pyramid base square, and X_0 the position of the cation-pyramid center of mass ($M''X_0 = M'X_0 = R$; see Fig. 17). For an asymmetric position X of the halogen at a distance ($R + z$) from the apex cation M'' , the local electric field is given by

$$\mathbf{E} = \left(\frac{Ze}{(R+z)^2} - 4 \frac{Ze}{(R \cos \Phi_0)^2 + (R \sin \Phi_0 - z)^2} \sin \Phi \right) \frac{\mathbf{z}}{z}, \quad (\text{B1})$$

where Ze is the charge of the anion and Φ the (\mathbf{MX} , \mathbf{MP}) angle. The first term of Eq. (B1) corresponds to the electric field on the halogen due to the M'' cation, and, for the second term, to the electric field due to the $4M'$ cations.

For $z=0$ ($\Phi = \Phi_0$); $\mathbf{E} = \mathbf{0}$, which leads to $\Phi_0 = \arcsin(1/4)$. For small z (for BaFI, the most layered compounds of the three studied, $z \sim 0.1 \text{ \AA} \ll R \sim 3.6 \text{ \AA}$), one can approximate Φ to Φ_0 in Eq. (B1). We obtain

$$\mathbf{E} = Ze \left(\frac{1}{(R+z)^2} - \frac{1}{R^2 - \frac{Rz}{2} + z^2} \right) \frac{\mathbf{z}}{z}. \quad (\text{B2})$$

By analogy with Eq. (7), the constant C can therefore be expressed as function of z :

$$C = \frac{R^4}{2} \left(\frac{1}{(R+z)^2} - \frac{1}{R^2 - \frac{Rz}{2} + z^2} \right)^2, \quad (\text{B3})$$

which, in the approximation of small z , leads to

$$C \approx \frac{25}{8} \left(\frac{z}{R} \right)^2. \quad (\text{B4})$$

The evolution of C as a function of z is given in Fig. 18, showing the increase of C for an asymmetric position of the halogen atom around the cation pyramid.

*Electronic address: fad@pmc.jussieu.fr

- ¹B. Liebich and D. Nicollin, *Acta Crystallogr., Sect. B: Struct. Crystallogr. Cryst. Chem.* **33**, 2970 (1977).
- ²M. Sauvage, *Acta Crystallogr., Sect. B: Struct. Crystallogr. Cryst. Chem.* **30**, 2786 (1974).
- ³H. P. Beck, *J. Solid State Chem.* **17**, 275 (1976).
- ⁴M. Pasero and N. Perchiazzi, *Miner. Mag.* **60**, 833 (1996).
- ⁵NBS Monogr. **25**, Sec. 10, 26 (1972); **25**, Sec. 13, 25 (1976).
- ⁶F. Hulliger, *Structural Chemistry of Layer-Type Phases* (Reidel, Dordrecht, 1975), pp. 258–264.
- ⁷K. Tkahashi, J. Miyahara, and Y. Shibahara, *Electrochem. Soc. Interface* **132**, 1492 (1985).
- ⁸Y. R. Shen, T. Gregorian, and W. B. Holzapfel, *High Press. Res.* **7**, 73 (1992).
- ⁹F. Datchi, PhD thesis, University of Paris, 1997.
- ¹⁰Y. R. Shen, U. Englisch, L. Chudinovskikh, F. Porsch, R. Haberkorn, H. P. Beck, and W. B. Holzapfel, *J. Phys.: Condens. Matter* **6**, 3197 (1994).
- ¹¹F. Decremps, M. Fischer, A. Polian, and M. Sieskind, *High Temp.-High Press.* **30**, 235 (1998).
- ¹²K. R. Balasubramanian, T. M. Haridasan, and N. Krishnamurthy, *Chem. Phys. Lett.* **67**, 530 (1979).
- ¹³G. R. Thompson and J. Turk, *Modern Physical Geology*, 2nd ed. (Saunders College, New York, 1997), p. 50.
- ¹⁴M. Sieskind, M. Ayadi, and G. Zachmann, *Phys. Status Solidi B* **136**, 489 (1986).
- ¹⁵R. Letoullac, J. P. Pinceaux, and P. Loubeyre, *High Press. Res.* **1**, 77 (1988).
- ¹⁶J. D. Barnett, S. Block, and G. J. Piermarini, *Rev. Sci. Instrum.* **44**, 1 (1973).
- ¹⁷A. Boulouf and D. Louer, *J. Appl. Crystallogr.* **24**, 987 (1991).
- ¹⁸N. Subramanian, N. V. Chandra Shekar, P. Ch. Sahu, Mohammad Yousuf, and K. Govinda Rajan, *Phys. Rev. B* **58**, R555 (1998).
- ¹⁹F. Decremps, M. Fischer, A. Polian, J. C. Chervin, and M. Sieskind (unpublished).
- ²⁰F. Birch, *J. Geophys. Res.* **57**, 227 (1952).
- ²¹F. Birch, *J. Geophys. Res.* **83**, 1257 (1978).
- ²²F. Decremps, M. Fischer, A. Polian, and M. Sieskind, *Eur. Phys. J. B* **5**, 7 (1998).
- ²³G. Kalpana, B. Palanivel, and I. B. Shameem Banu, *Phys. Rev. B* **56**, 3532 (1997).
- ²⁴M. Sieskind, A. Polian, M. Fischer, and F. Decremps, *J. Phys. Chem. Solids* **59**, 75 (1998).
- ²⁵M. Fischer, A. Polian, and M. Sieskind, *J. Phys.: Condens. Matter* **6**, 10 407 (1994).
- ²⁶M. Fischer, M. Sieskind, A. Polian, and A. Lahmar, *J. Phys.: Condens. Matter* **5**, 2749 (1993).
- ²⁷F. Decremps, M. Fischer, A. Polian, J. P. Itié, and M. Sieskind, *Eur. Phys. J. B* (to be published).
- ²⁸M. Born and K. Huang, *Dynamical Theory of Crystal Lattices* (Oxford Univ., London, 1954).
- ²⁹M. Sieskind and J. Morel (unpublished).
- ³⁰J. R. Tessman and A. H. Kahn, *Phys. Rev.* **92**, 890 (1953).
- ³¹E. F. Bertaut, *C. R. Acad. Sci., Ser. II: Mec., Phys., Chim., Sci. Terre Univers* **302**, 285 (1986).
- ³²C. Haas, in *Proceedings of the Yamada Conference IV*, edited by Y. Nishina [*Physica B* **105**, 305 (1981)].
- ³³E. F. Bertaut, *J. Phys. (Paris)* **39**, 1331 (1978).
- ³⁴A. Polian, PhD thesis, University of Paris, 1981.
- ³⁵J. C. Chervin, B. Canny, J. M. Besson, and Ph. Pruzan, *Rev. Sci. Instrum.* **66**, 2595 (1995).
- ³⁶J. W. Otto, J. K. Vassiliou, and G. Frommeyer, *Phys. Rev. B* **57**, 3253 (1998).
- ³⁷J. M. Léger, A. M. Redon, and C. Chateau, *Phys. Chem. Miner.* **17**, 161 (1990).